ISSN 0915-633X

NATIONAL INSTITUTE FOR FUSION SCIENCE

Impulsive Nature in Collisional Driven Reconnection

H. Kitabata, T. Hayashi, T. Sato and
Complexity Simulation Group

(Received - Nov. 6, 1995)

NIFS-385 Nov. 1995

RESEARCH REPORT
NIFS Series

NAGOYA, JAPAN

Impulsive Nature in Collisional Driven Reconnection

Hideyuki KITABATA

Department of Fusion Science,

The Graduate University for Advanced Studies, Nagoya 464-01, Japan.

Takaya HAYASHI, Tetsuya SATO

and

Complexity Simulation Group[†]

Theory and Computer Simulation Center,

National Institute for Fusion Science, Nagoya 464-01, Japan.

Abstract

Compressible magnetohydrodynamic simulation is carried out in order to investigate energy relaxation process of the driven magnetic reconnection in an open finite system through a long time calculation. It is found that a very impulsive energy release occurs in an intermittent fashion through magnetic reconnection for a continuous magnetic flux injection on the boundary. In the impulsive phase, the reconnection rate is remarkably enhanced up to more than ten times of the driving rate on the boundary.

Keywords: Impulsive nature, Driven reconnection, Relaxation process, Magnetic island, Fast reconnection, Intermittency, Plasma jet

---

[†]R.Horiuchi, K.Watanabe, A.Kageyama, T.Watanabe, Y.Todo, H.Takamaru

I. INTRODUCTION

Recently, it has been revealed through a simulation study that an open system where a flux of free energy is continuously supplied exhibits noteworthy characteristics such as intermittency and recurrency.[1] The study was made on global scale nonlinear behavior in a resistive magnetohydrodynamic (MHD) plasma. Here we suppose that intermittency would arise in various classes of nonlinear responses in a complex system of plasma. In this paper, having in mind a similar expectation, we focus on an important elementary process in a resistive MHD plasma, that is, magnetic reconnection. With this expectation, we revisited compressible, resistive MHD simulations of the driven magnetic reconnection.[2] Another expectation is that existence of such intermittent nature in reconnection, if any, may be directly related with a possible mechanism of what is called ' fast reconnection '. Magnetic reconnection has been thought to play a fundamental role in the dynamics of various impulsive magnetic phenomena, for instance, the fast crash in sawtooth oscillations observed in tokamak plasmas and an impulsive energy release observed in the solar flare. However, it has not yet been clarified how such fast reconnection occurs. In recent years several authors, such as Drake and Kleva[3], Wesson[4], and Aydemir[5], have attempted to explain the ' fast reconnection ' by including various terms, such as the electron inertia and electron pressure terms, in the generalized Ohm's law of basic MHD equations. In this paper, we examine whether or not the fast reconnection can occur in a ' pure ' resistive MHD plasma where the Ohm's law in its simplest form is used.

II. SIMULATION MODEL

In order to investigate thoroughly the driven magnetic reconnection process in an open system, we carry out a very long time scale calculation. The simulation model is based on 2-D compressible resistive MHD equations. In the previous paper[2], the dynamics of the driven magnetic reconnection was studied by employing what is called the anomalous resis-

tivity model, where the resistivity was assumed to be enhanced as a function of the plasma current. In this paper, we adopt the simplest resistivity model, i.e., a uniform model. The code we use has a high resolution which includes more than ten grid points across the diffusion region (current layer) around the X-point. Here we note that the compressibility of the plasma plays a crucial role in a dynamic process of the MHD driven reconnection as was already indicated in the previous paper[6]. Also we note that realization of a very long time scale calculation is essential in revealing the energy relaxation process in the MHD driven reconnection.

The governing equations are the following compressible MHD equations ;

$$\rho\frac{d\boldsymbol{v}}{dt} = -\nabla P + \boldsymbol{j}\times\boldsymbol{B} + \nu\left(\nabla^2\boldsymbol{v} + \frac{1}{3}\nabla\left(\nabla\cdot\boldsymbol{v}\right)\right) \tag{2.1}$$

$$\frac{\partial\boldsymbol{B}}{\partial t} = -\nabla\times\boldsymbol{E} \tag{2.2}$$

$$\frac{dP}{dt} = -\gamma P\nabla\cdot\boldsymbol{v} + (\gamma-1)\left(\eta\boldsymbol{j}^2 + \Phi\right) \tag{2.3}$$

$$\frac{\partial\rho}{\partial t} = -\nabla\cdot(\rho\boldsymbol{v}) \tag{2.4}$$

$$\mu_0\boldsymbol{j} = \nabla\times\boldsymbol{B} \tag{2.5}$$

$$\boldsymbol{E} = -\boldsymbol{v}\times\boldsymbol{B} + \eta\boldsymbol{j} \tag{2.6}$$

$$\Phi = 2\nu\left(e_{ij}e_{ij} - \frac{1}{3}\left(\nabla\cdot\boldsymbol{V}\right)^2\right) \tag{2.7}$$

$$e_{ij} = \frac{1}{2}\left(\frac{\partial v_i}{\partial x_j} + \frac{\partial v_j}{\partial x_i}\right) \tag{2.8}$$

$$\eta = \text{const.} \tag{2.9}$$

The most notation is conventional; η is the resistivity, ν is the viscosity, γ is the adiabatic constant, and μ_0 is the permeability.

Since we have confirmed that the main results shown in this paper are not affected by the detailed structure of the plasma density ρ, we present here the results of simulation in which ρ is assumed constant instead of solving (2.4). The nature of the compressibility is expressed in the pressure equation, (2.3).

The initial condition is given by the Harris-type equilibrium,

$$B_x(y) = B_{x0} \tanh(y/L) \tag{2.10}$$

$$P(y) = P_0 \mathrm{sech}^2(y/L) + P_1 \tag{2.11}$$

$$j(y) = j_0 \mathrm{sech}^2(y/L) \tag{2.12}$$

$$B_z(y) = B_{z0} \tag{2.13}$$

$$\rho = \rho_0 \tag{2.14}$$

where B_{x0}, B_{z0} and ρ_0, P_1 are constant, and $P_0 = B_{x0}^2/2\mu_0$, $j_0 = B_{x0}/\mu_0 L$.

In the following we describe variables in the normalized form, where the normalization units for several quantities are given in Table I. The calculations are confined to the x-y plane, $-60 \leq x \leq 60$ and $-6 \leq y \leq 6$, on a Cartesian grid with $N_x \times N_y = 188 \times 122$ grid points, which was proved to be fine enough by performing a finer resolution $N_x \times N_y = 288 \times 222$, and $\partial/\partial z$=zero is assumed. The mirror symmetry is assumed for both x and y axes. The spatial derivative is approximated by a two point central difference, and the fourth order Runge-Kutta-Gill scheme is used for time advancing. The simulation box is illustrated in Fig.1. We assume that the driving plasma flow is injected symmetrically by imposing an

electric field E_{z0} on the input boundaries ($y = \pm 6$). E_{z0} is peaked at $x = 0$ on the input boundaries. On the other boundaries, $x \leq -50$ and $x \geq 50$, an artificial absorbing zone is installed to suppress spurious reflection of physical waves[2].

III. SIMULATION RESULT

Surprisingly and in contrast to the conventional simulations, long time scale calculations have disclosed intermittent and very impulsive phenomena in the energy relaxation process of the driven magnetic reconnection. Figure 2 presents the highlights of the simulation results, where the temporal evolution of the electric field E_z at the X-point is shown. Recalling that E_z at the X-point is equivalent to the rate of magnetic flux change on the X-point, the reconnection rate is found to be impulsively and intermittently intensified. It is usually believed that in the MHD driven reconnection the saturated level of the reconnection rate must be as large as the external driving electric field (dashed line; $Ez_0 = 0.06$) that is expressed as $\boldsymbol{v} \times \boldsymbol{B}$ on the boundary, or at most the peak rate is two times of the driving rate[7]. Most previous simulations have not been continued far beyond the time when E_z at the X-point has first reached at a level of the driving field, partly because numerical instabilities usually prevent continuation of long time-scale computations. By developing a stable code in this study, it becomes possible to calculate long enough. In Fig.2, it is seen that E_z drops off soon after the saturation at $T \sim 600\tau_A$, but what should be noted is that at $T \sim 2000\tau_A$ E_z increases rapidly as an impulsive fashion and the peak intensity attains more than ten times of the driving rate on the boundary. Interestingly, such an impulsive change is repeated intermittently. The appearance of the strong peak of E_z at the X-point in the impulsive phase indicates a very fast reconnection. It is noted that a dynamical change of the magnetic structure happens rapidly in the impulsive phase through the fast reconnection.

Figure 3 shows the time evolution of the maximum value of the plasma jet (V_{xmax} at y=0). These peaks coincide with those of E_z at the X-point, and each maximum peak exceeds ten

times of the Alfven velocity defined by the initial condition. Figure 4(a) shows the temporal evolution of the Joule heating and the plasma acceleration integrated over the whole region, $\int \eta j^2 dxdy$ and $\int \boldsymbol{v} \cdot (\boldsymbol{j} \times \boldsymbol{B})\, dxdy$, respectively. The former is the rate of energy conversion from the magnetic to plasma thermal energy through the ohmic heating in the system (ηj^2), and the latter is the conversion rate to the kinetic energy through the work of the Ampere force ($\boldsymbol{j} \times \boldsymbol{B} \cdot \boldsymbol{v}$). It is perceived that anomalous dissipation is enhanced remarkably at the impulsive phase in accordance with the rapid change of the magnetic structure. It is also noteworthy that the dissipation is enhanced mainly through the plasma acceleration rather than the ohmic heating. Figure 4(b) shows the temporal evolution of the rate of change of the total magnetic energy stored in the system dW/dt, where $W = \int \frac{B^2}{2} dxdy$. It appears that the magnetic energy injected from outside is gradually accumulated in the system in the slow reconnection phase which is followed by the impulsive phase when the stored magnetic energy is released rapidly through conversion to the kinetic and thermal energy. A similar process is repeated.

What does happen in the impulsive phase? Figure 5 shows the behavior in the long time scale of the magnetic field lines. Magnetic reconnection has developed sufficiently by the external driving plasma flow at $T = 200\tau_A$. At $T \sim 500\tau_A$ a magnetic island happens to be born in the center of the system region, and grows up gradually until $T \sim 1850\tau_A$. Then at $T = 1958\tau_A$ the crash of the island breaks out, whereby the island is divided into two plasmoids. After that, it is found that a new magnetic island is formed again in the center of the system region.

Next, we shall focus our attention on the detailed process near the crash. Figure 6 shows the behavior in the impulsive phase of the magnetic field lines. Note that a significant change occurs in the magnetic structure in a very short period. At $T = 1953\tau_A$ the magnetic island which has grown enough is compressed by the input flow. And at $T = 1958\tau_A$ the plasmoids created by the crash run away and immediately disappear by reconnection with magnetic field lines in the front. The new island is born soon after the crash ($T = 1960\tau_A$), and grows up ($T = 1965\tau_A$). Figure 7 shows the behavior of the plasma flow in the impulsive phase.

It is found that a strong plasma flow is excited explosively after the crash ($T = 1958\tau_A$). Shown in Figure 8 is the bird's-eye view of the intensity of the vertical current J_z in the impulsive phase. Here the intensity of J_z in the initial condition is too small to be visible in the scale of this plot. $T = 1850\tau_A$ is the time when the island grows to its biggest size, and then immediately the first crash occurs. The view at $T = 1958\tau_A$ displays J_z at the instance of the crash, and the peak with strong intensity which appears in the vicinity of the center causes an impulsive enhancement of E_z through ηj. At this moment the peak intensity of J_z is grown up to 141, which is fairly large compared with the initial value, namely, 1. Shown in the views at $T = 1960\tau_A$ and $T = 1965\tau_A$ are the behaviors of J_z around the new island which is created soon after the crash.

Figure 9 shows the bird's-eye view of E_z at the same moments as shown in Fig.8. It should be noted again that the intensity of E_z given on the boundary is too small to be visible in the plots. E_z at $T = 1958\tau_A$, coincident with the crash time, is much higher in intensity than E_z at $T = 1850\tau_A$. It is quite surprising that E_z in the outflow region with the peak value of 11.6 significantly exceeds E_z near the X-point with the value of 0.7 which is mainly sustained by the ohmic current J_z shown in Fig.8. It is found that such strong E_z in the outflow region is caused by the $\boldsymbol{v} \times \boldsymbol{B}$ term because a strong plasma jet is generated as shown in Fig.7. This result again indicates that the magnetic energy is predominantly dissipated into the form of the plasma flow energy. Such strong E_z is enhanced further at $T = 1960\tau_A$ with the peak value of 12.8. The inversion of the sigh of E_z observed in the plots are due to the fact that the sign of B_y in front of the plasmoid is opposite to that behind. It is observed that the strong E_z value remains for some time.

What causes such an impulsive nature? To answer this question, we have examined the dependence on two parameters, namely, the size of the inflow region for the driving flow (X_{size} ; the width in x direction) on the boundary and the intensity of the driving flow. Figure 10 shows the dependence on X_{size}, where the upper is for a narrow driving region ($X_{size} = 25$) and the lower is for a wider one ($X_{size} = 50$). Other conditions are the same as those shown in Table 2. It is seen that the maximum peak intensity of E_z is much higher

for the larger X_{size} case than the small one. In the smaller X_{size} case, the first crash of the island occurs at T $\sim 1000\tau_A$, while it does at T $\sim 2000\tau_A$ for the larger X_{size} case. Thus, the crash time is delayed doubly as the size of the inflow region size is doubled. We plot in Fig.11 the time profile of the width of the magnetic island, where the width is defined as the half length of the island in x direction. This plot indicates that in the earlier phase islands grow rapidly, but the growth is reduced to a much lower level quickly. Comparison of Fig.10 (lower) with Fig.11 indicates that crash is always triggered as soon as the size of island reaches to a critical value. Aiming at searching for the reason of the island crash, we examine the behavior of E_z at the edge of the island. As is seen in Figure 12, E_z at the edge of the island decreases before occurrence of the first crash, and almost vanishes at $T \sim 1850\tau_A$, when the size of island becomes maximum. The reconnection point at the island edge moves outwards in the x direction as the island grows, while the driving flow from the input boundary is limited in a certain x region. Accordingly, when the reconnection point goes beyond the driving region, no more magnetic flux is supplied into the magnetic island through the edge reconnection point, thus, the island growth is stopped. At this point, compression of the island by the driving flow at the central part surpasses the swelling of the island by the flux supply through the edge reconnection point. These considerations conclude that the island growth is maintained by the magnetic flux supplied by the driving flow through the edge reconnection point, not by a spontaneous instability like the tearing instability as was concluded by Fu and Lee[7]. (Biskamp[8] has also observed formation of islands in a current layer, but its impulsive nature is not explicitly discussed.) Figure 13 shows the dependence of the peak intensity of the impulse on E_{z0}, i.e., the intensity of the driving plasma flow. The triangle symbol is for the case with $X_{size} = 50$, the circle represents the case with $X_{size} = 25$. The peak intensity increases in proportion to E_{z0} for both cases. It should be noted, especially in $E_{z0} \leq 0.01$, that an impulsive nature is lost and the saturation rate amounts nearly to the driving one. The case of $E_{z0} \leq 0.01$ is displayed in Figure 14 which shows temporal evolution of the E_z at the X-point. E_z exhibits an almost steady behavior except for some variations in the earlier phase. Let us then examine the

dependence of the duration of an impulse on E_{z0}. Figure 15 shows its dependence. The duration of an impulse is defined as the time that the condition of E_z (at X-point) $\geq E_{z0}$ is satisfied in the impulsive phase. The symbols are equivalent to those in Fig.13. It is found that the duration decreases as E_{z0} increases. In this regard, it should be recalled that the intensity of impulse increases as E_{z0} increases.

IV. CONCLUSION

We have studied the relaxation process of driven magnetic reconnection by performing a long simulation run. By making a long time scale calculation, we discovered extremely intensive impulsive reconnection and intermittent nature of bursts in the long time behavior of the driven magnetic reconnection. The reconnection rate reaches to an extremely large value, say, more than ten times of the driving rate in a pure resistive MHD, without invoking any electron inertia or electron pressure effects in the generalized Ohm's law. Through this impulsive reconnection, the stored magnetic energy is mainly converted to the plasma flow energy. Examination of the dependence of the impulsive reconnection on the two external parameters, i.e., the intensity and the inflow size of the driving plasma flow, has disclosed that the inflow size of the driving flow determines the onset time of crash. The peak intensity of an impulse is proportioned to the size, as well as the intensity, of the driving flow. On the other hand, the width of an impulse is shortened as the driving flow is increased but independent of the size of the driving flow. These behaviors conclude that very fast reconnection can take place naturally in a driven process and that it occurs in a very impulsive and intermittent fashion. The reconnection rate is intensified much larger than the surrounding driving flow at its peak.

ACKNOWLEDGMENTS

This work is carried out by using the Advanced Computing System for Complexity Simulation (NEC SX-3/24R) at NIFS (National Institute for Fusion Science).

[1] H. Amo, T. Sato, A. Kageyama, and the Complexity Simulation Group, Phys. Rev.E 51, R3838-R3841 (1995).

[2] T. Sato and T. Hayashi, Phys. Fluids, 22, 1189–1201 (1979).

[3] J. F. Drake and R. G. Kleva, Phys. Rev. Lett. 66, 1458-1461 (1991).

[4] J. A. Wesson, Plasma Physics and Controlled Nuclear Fusion Research, 1990, Washington D.C., (IAEA, Vienna, 1991) 2, p79.

[5] A. Y. Aydemir, Phys. Fluids B, 4, 3469-3472 (1992).

[6] T. Sato, T. Hayashi, K. Watanabe, R. Horiuchi, M. Tanaka, N. Sawairi, K. Kusano, Phys. Fluids B, 4, 450–457, (1992).

[7] Z. F. Fu and L. C. Lee, J. Geophys. Res., 91, 13,373–13,383, (1986).

[8] D. Biskamp, Phys.Fluids, 29(5), 1520-1531, (1986).

FIGURE CAPTION

FIG. 1. Schematic illustration of the simulation box.

FIG. 2. Temporal evolution of electric field E_z at X-point where $E_{z0} = 0.06$, $X_{size} = 50$.

Fig. 3. Temporal evolution of the maximum velocity in the diffusion layer.

FIG. 4. Temporal evolution of the rate of energy change in the system ;

(a) Joule heating ηj^2 (dashed line), and plasma acceleration $\boldsymbol{j} \times \boldsymbol{B} \cdot \boldsymbol{v}$ (straight line).

(b) The conversion rate of total magnetic energy.

FIG. 5. The behaviors of magnetic field lines in the long time scale.

FIG. 6. The behaviors of magnetic field lines in the impulsive phase.

FIG. 7. The behavior of plasma flow in the impulsive phase.

FIG. 8. The bird's eye views of current J_z in the impulsive phase.

FIG. 9. The bird's eye views of electric field E_z in the impulsive phase.

FIG. 10. Difference in temporal evolution of E_z depending on the size of the inflow region X_{size} of the driving flow on the boundary. The upper is for $X_{size} = 25$, and the lower is for $X_{size} = 50$, where $E_{z0} = 0.06$.

FIG. 11. Temporal evolution of the half width of magnetic island in x direction where $E_{z0} = 0.06$, $X_{size} = 50$.

FIG. 12. The behavior of the X-point electric field at the edge of magnetic island is zoomed up before the occurence of the first crash where $E_{z0} = 0.06$, $X_{size} = 50$.

FIG. 13. The maximum peak intensity of impulse versus driving electric field E_{z0}

FIG. 14. Temporal evolution of electric field E_z at X-point where $E_{z0} = 0.01$, $X_{size} = 25$

FIG. 15. The duration of impulse versus driving electric field E_{z0}

TABLE CAPTION

TABLE 1. The normalization unit for several variables.

TABLE 2. The parameters for the typical calculation.

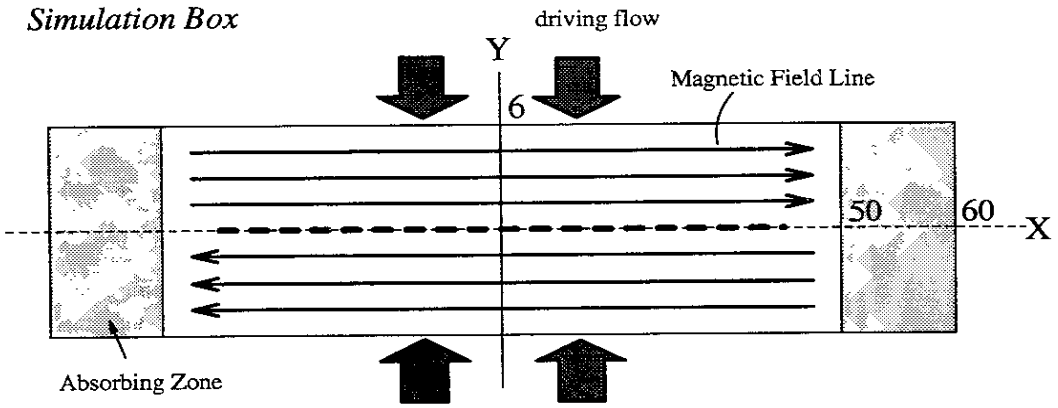

Fig.1

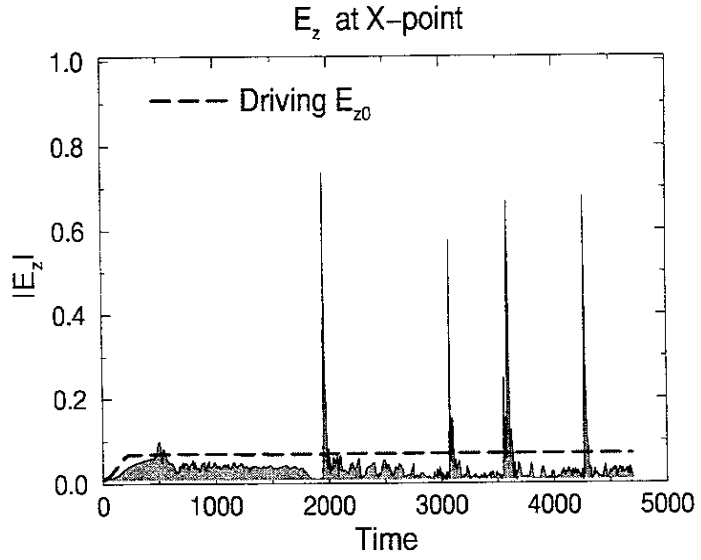

Fig.2

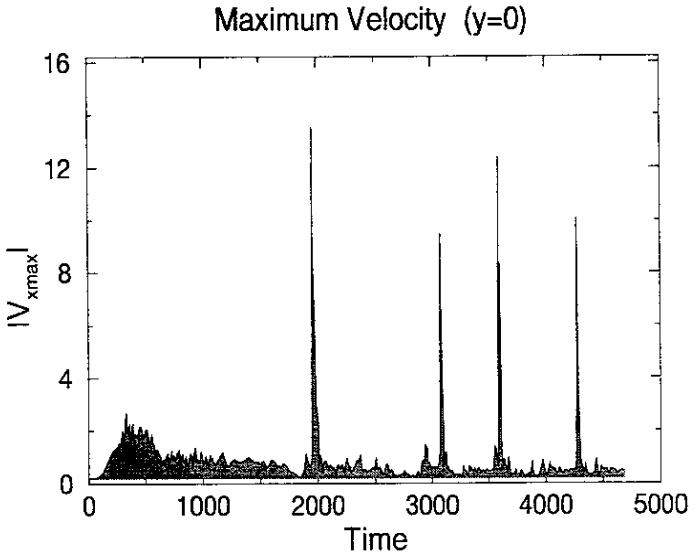

Fig.3

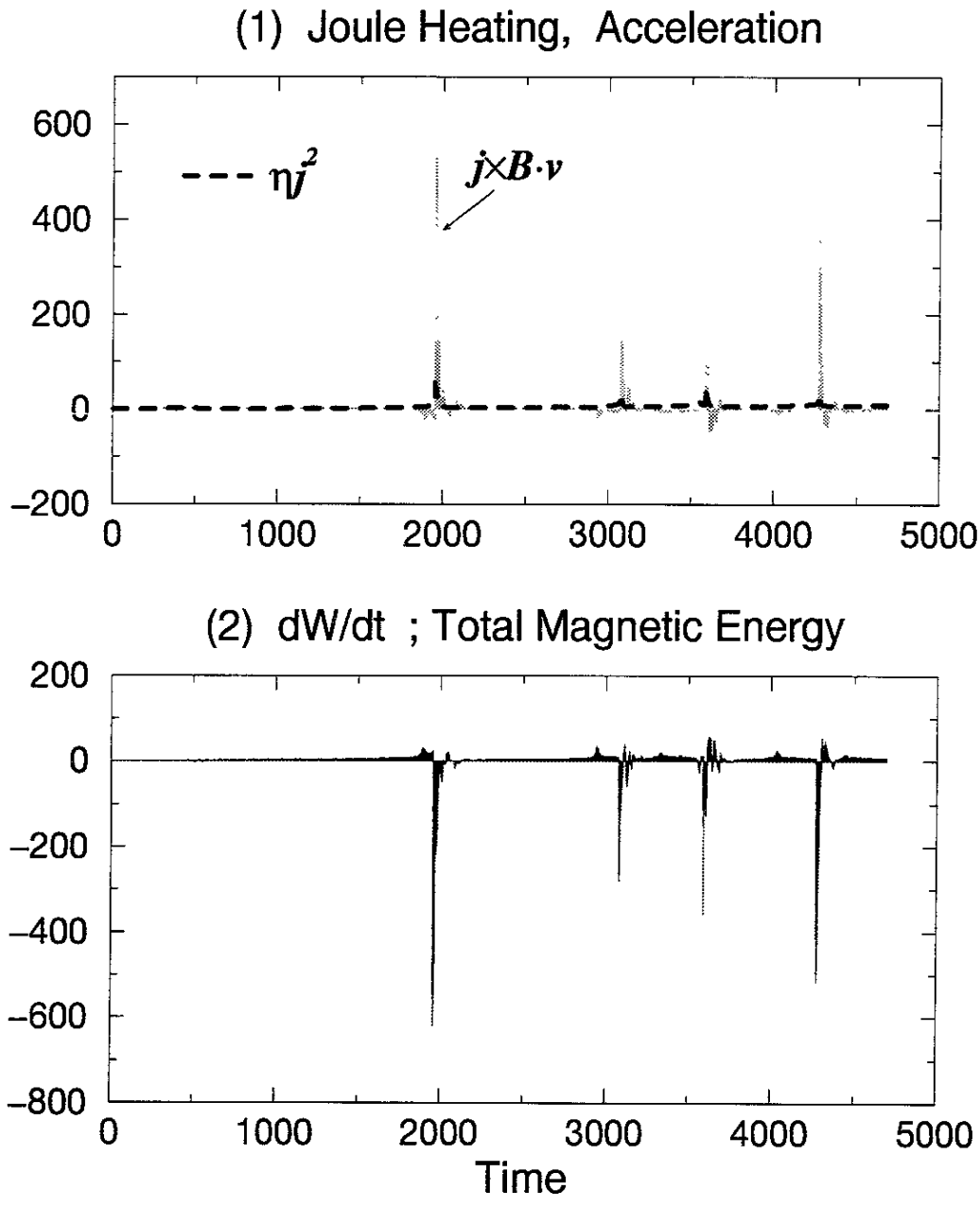
(1) Joule Heating, Acceleration
600
400
200
0
-200
ηj^2
$j \times B \cdot v$
0
1000
2000
3000
4000
5000
(2) dW/dt ; Total Magnetic Energy
200
0
-200
-400
-600
-800
0
1000
2000
3000
4000
5000
Time

Fig.4

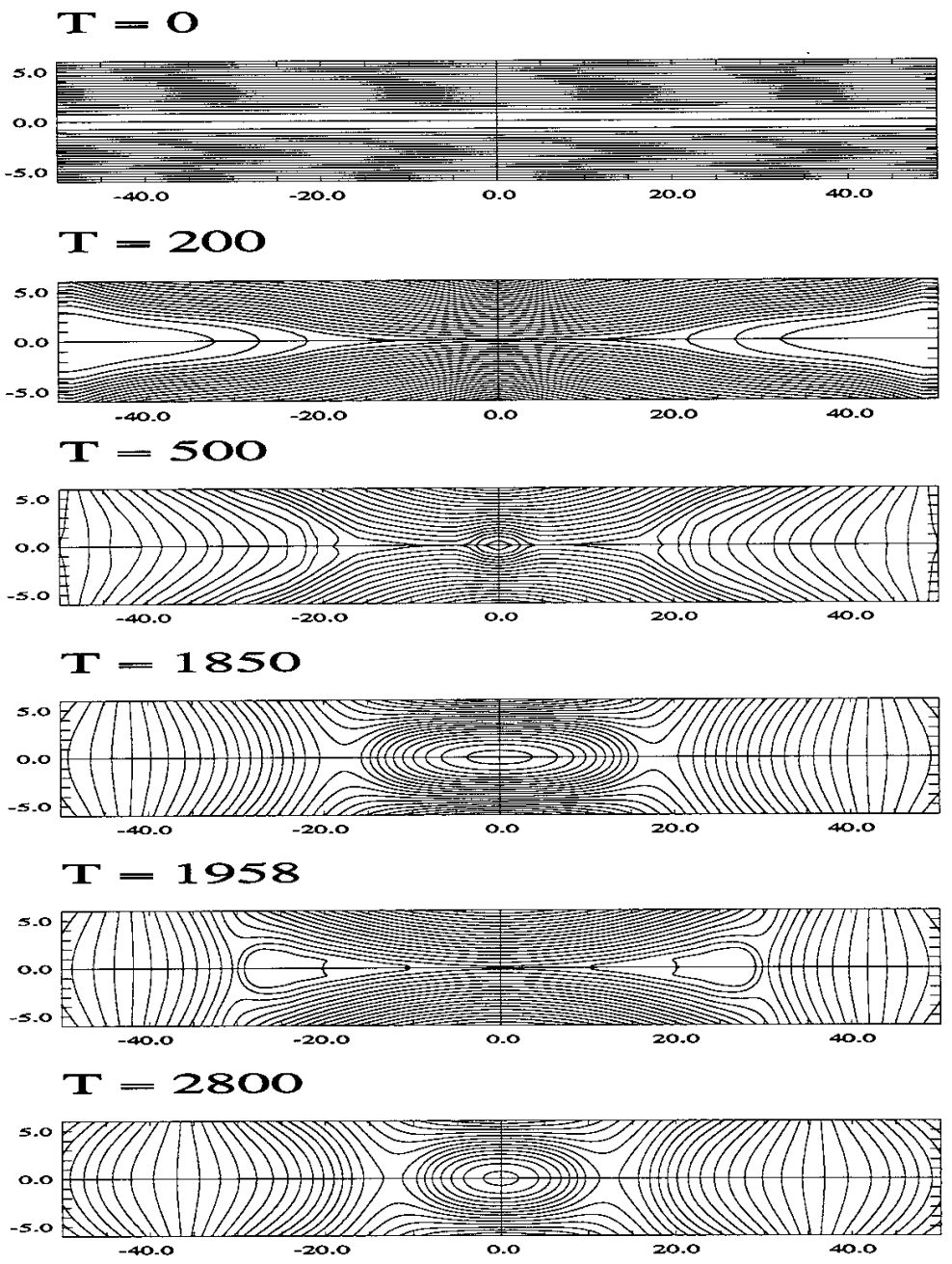

Fig.5

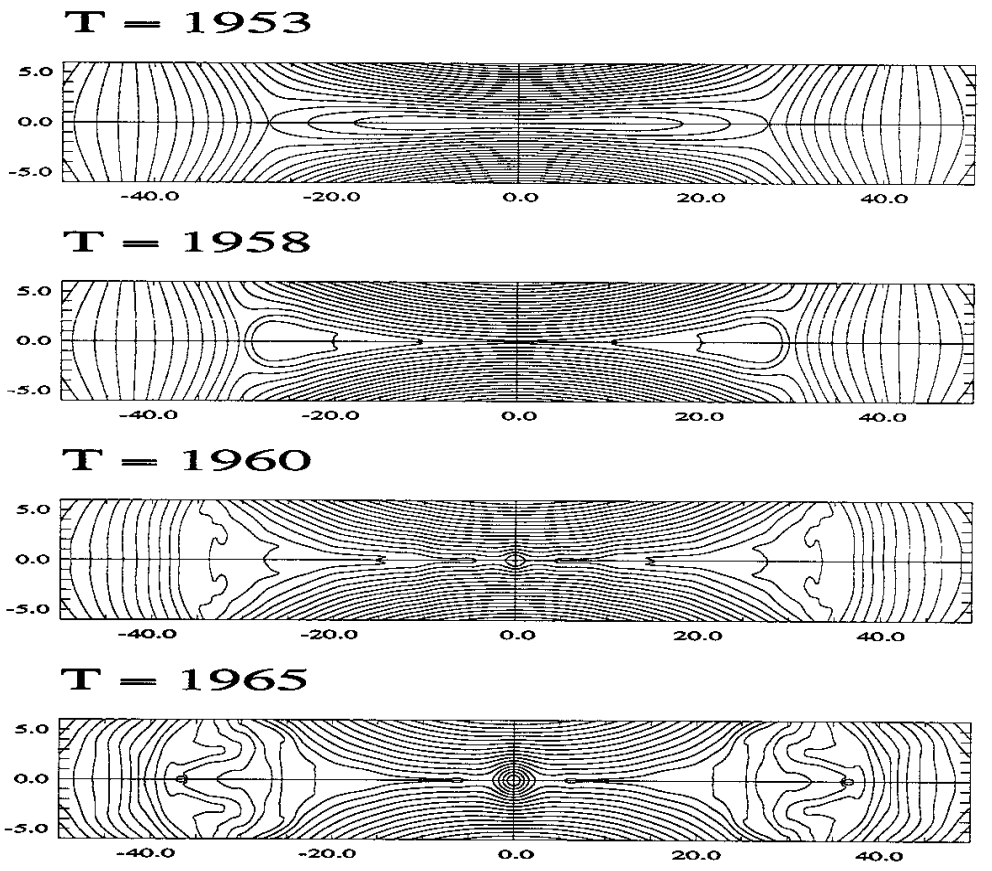
T = 1953
5.0
0.0
-5.0
-40.0
-20.0
0.0
20.0
40.0
T = 1958
5.0
0.0
-5.0
-40.0
-20.0
0.0
20.0
40.0
T = 1960
5.0
0.0
-5.0
-40.0
-20.0
0.0
20.0
40.0
T = 1965
5.0
0.0
-5.0
-40.0
-20.0
0.0
20.0
40.0

Fig.6

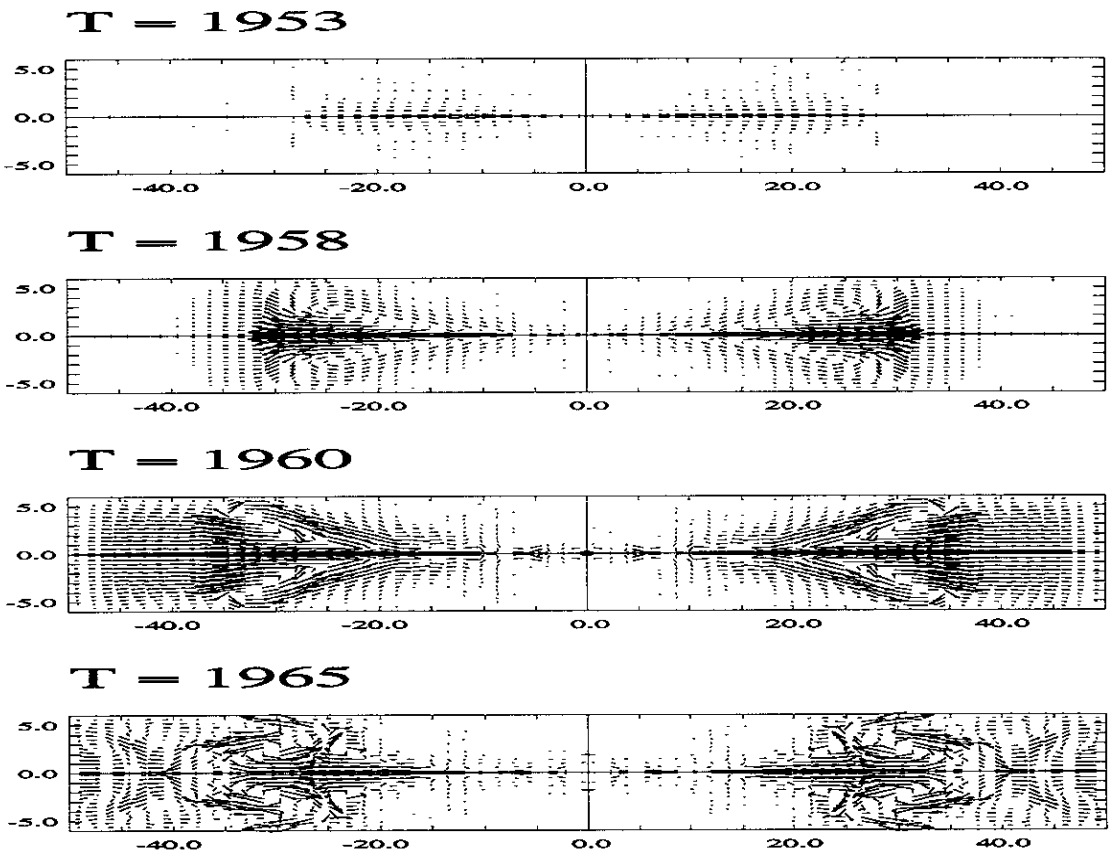
T = 1953
5.0
0.0
-5.0
-40.0
-20.0
0.0
20.0
40.0
T = 1958
5.0
0.0
-5.0
-40.0
-20.0
0.0
20.0
40.0
T = 1960
5.0
0.0
-5.0
-40.0
-20.0
0.0
20.0
40.0
T = 1965
5.0
0.0
-5.0
-40.0
-20.0
0.0
20.0
40.0

Fig.7

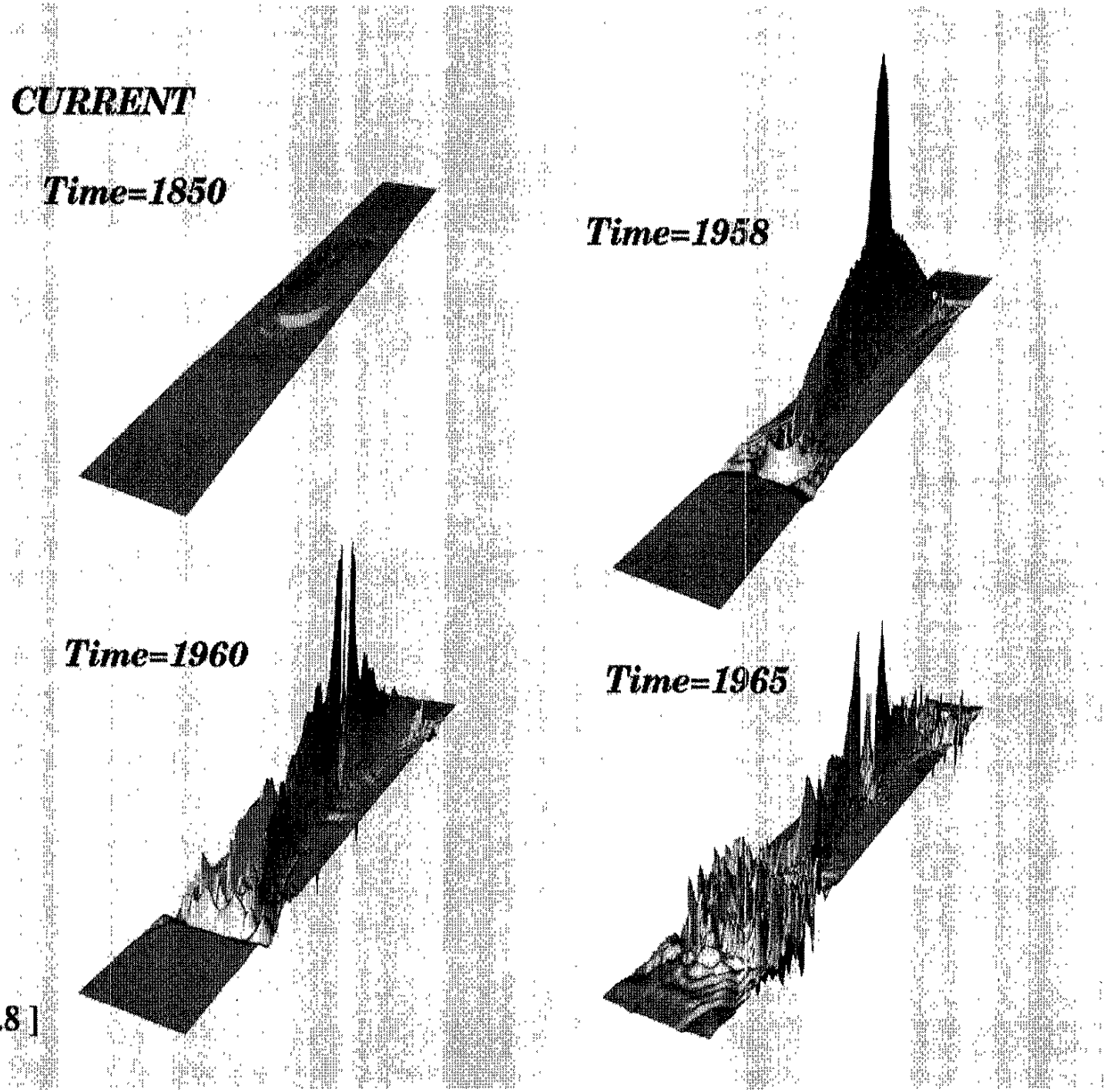

[Fig.8]

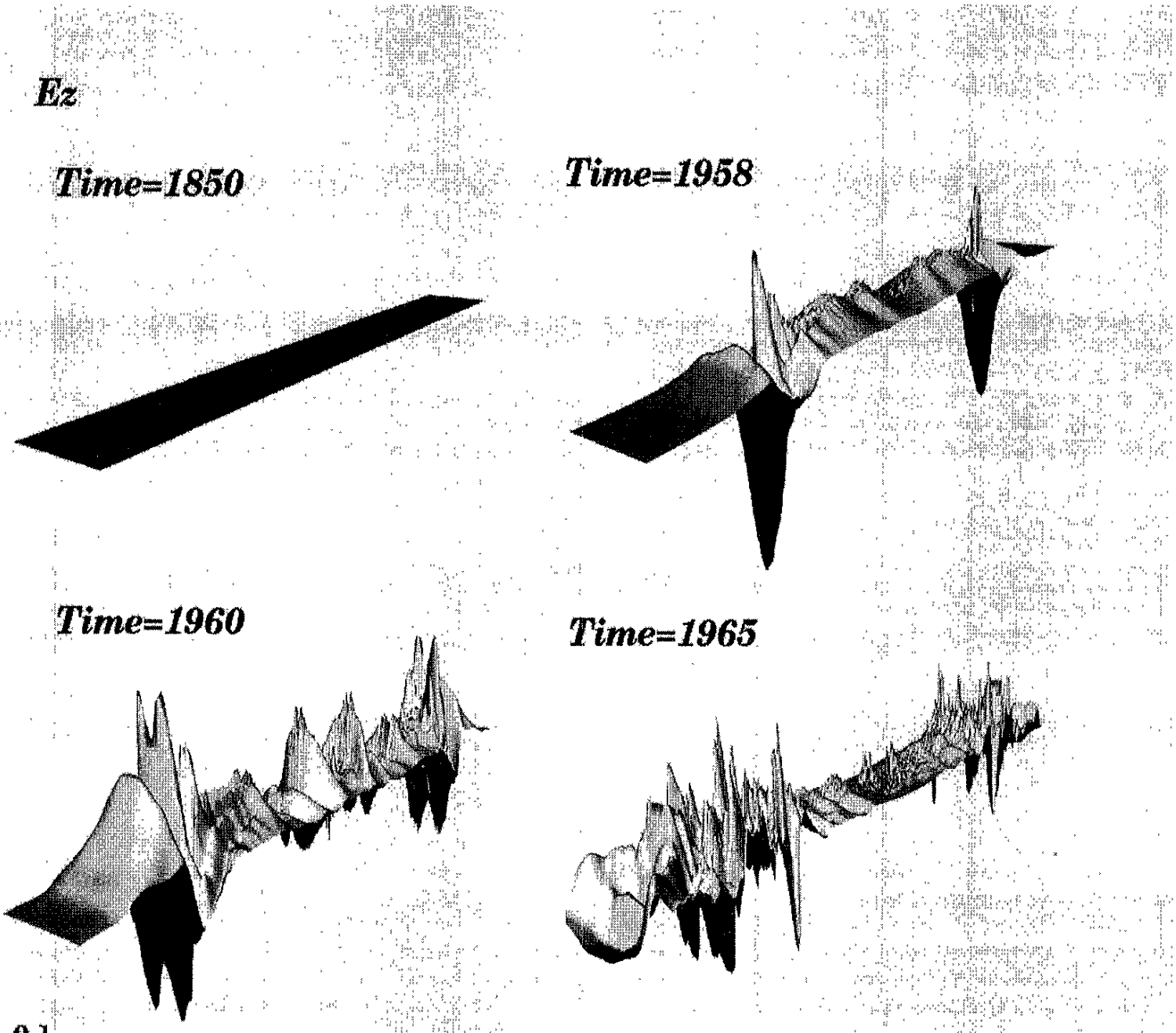

[Fig.9]

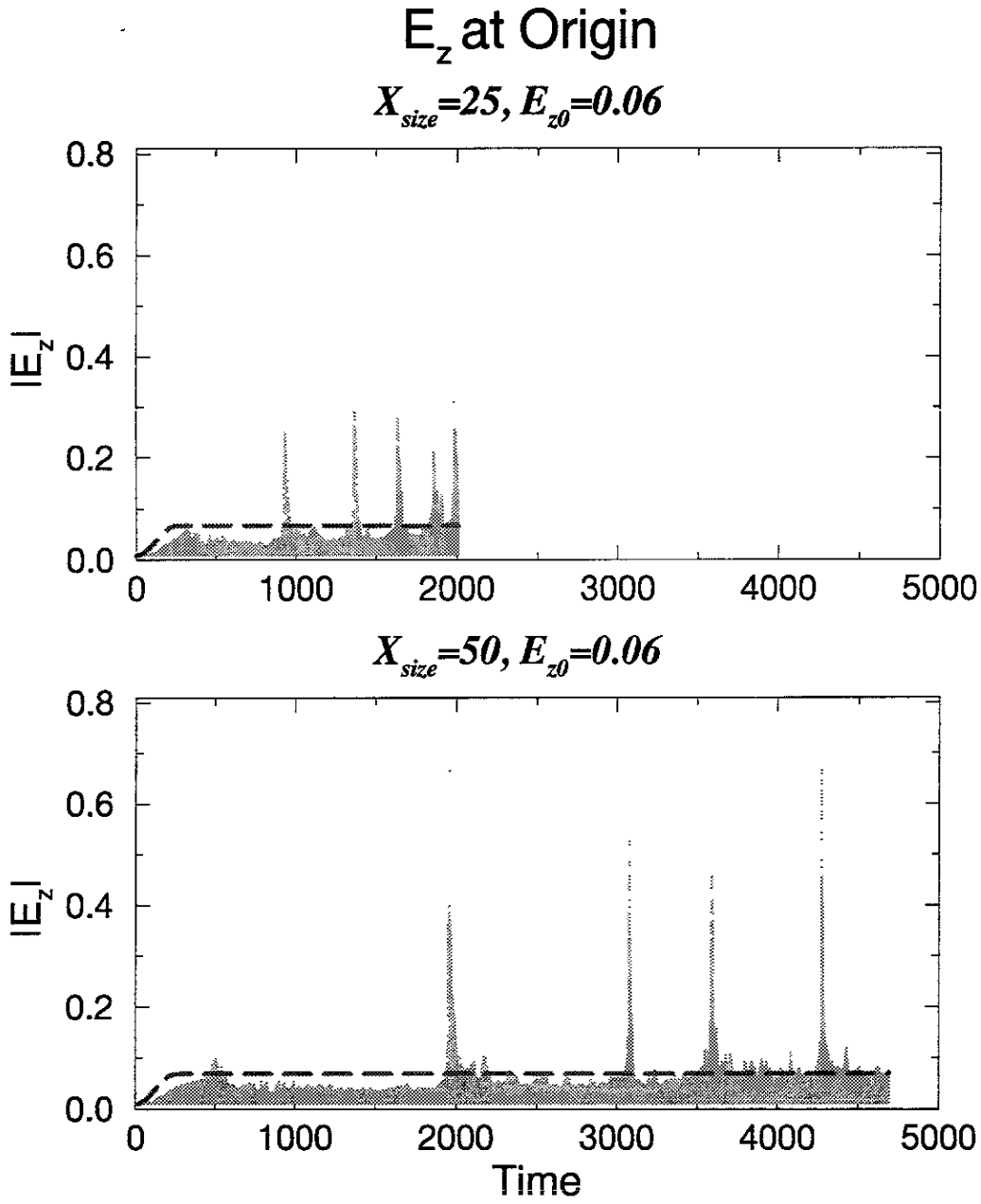
E_z at Origin
X_size=25, E_z0=0.06
|E_z|
0.8
0.6
0.4
0.2
0.0
0
1000
2000
3000
4000
5000
X_size=50, E_z0=0.06
|E_z|
0.8
0.6
0.4
0.2
0.0
0
1000
2000
3000
4000
5000
Time

Fig.10

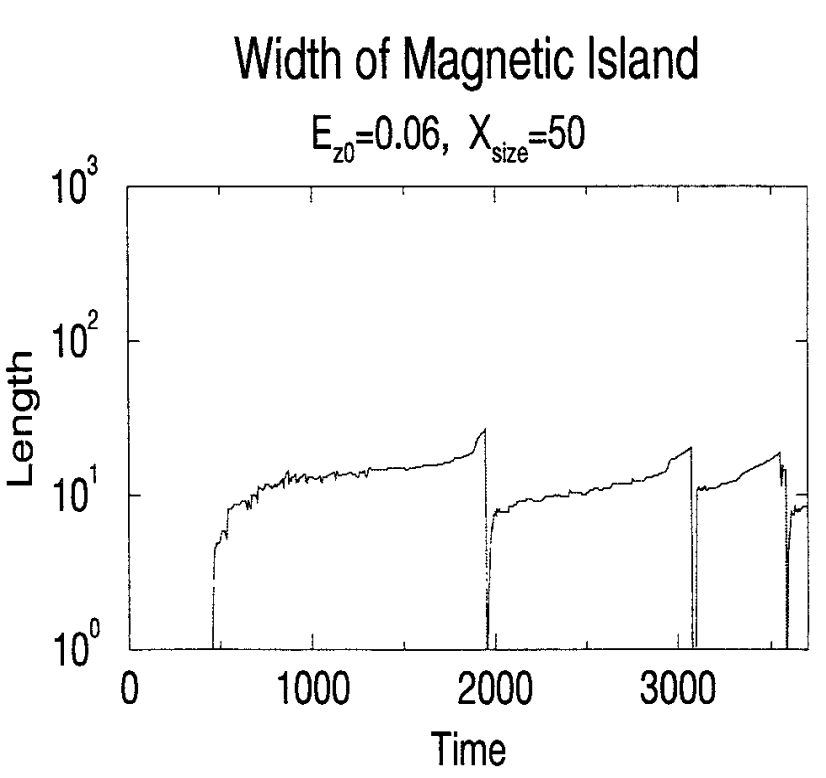
Width of Magnetic Island
E_{z0}=0.06, X_{size}=50
Length
10^3
10^2
10^1
10^0
0
1000
2000
3000
Time

Fig.11

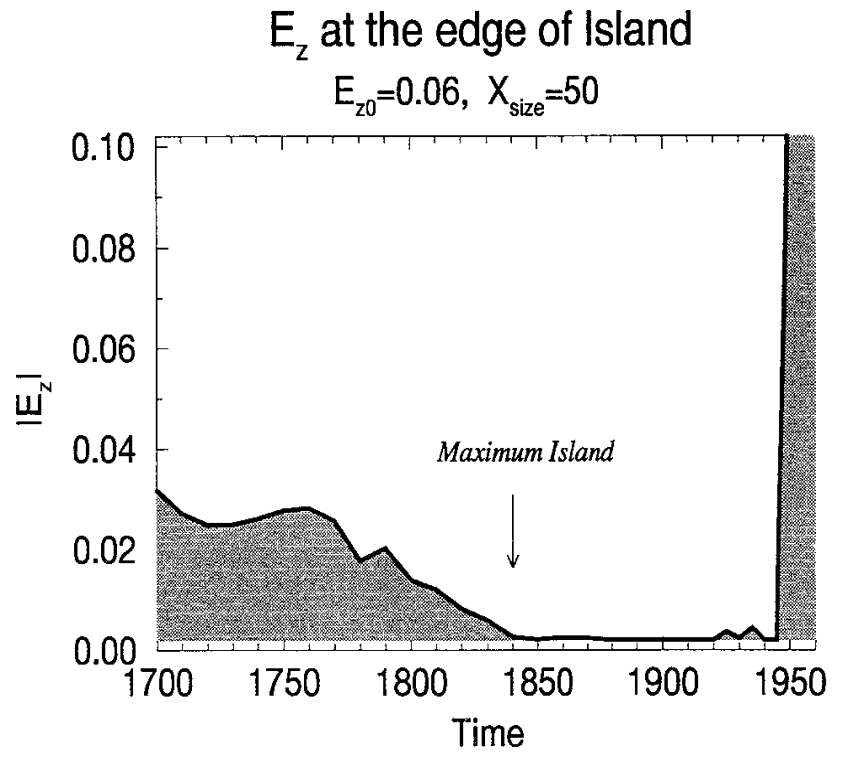
E_z at the edge of Island
E_{z0}=0.06, X_{size}=50
$|E_z|$
0.10
0.08
0.06
0.04
0.02
0.00
Maximum Island
1700
1750
1800
1850
1900
1950
Time

Fig.12

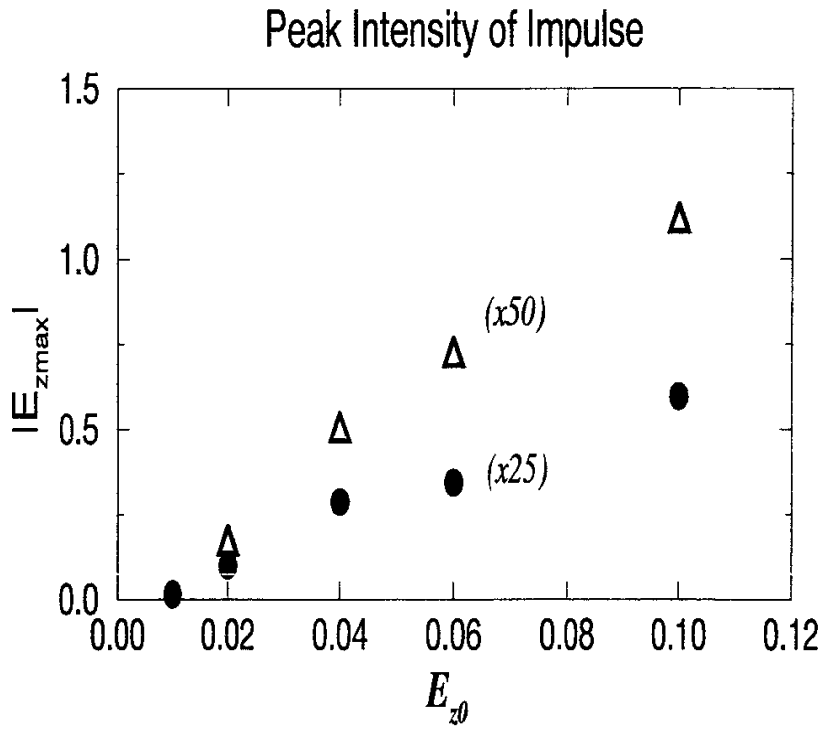
Peak Intensity of Impulse
1.5
1.0
0.5
0.0
|E_zmax|
(x50)
(x25)
0.00
0.02
0.04
0.06
0.08
0.10
0.12
E_z0

Fig.13

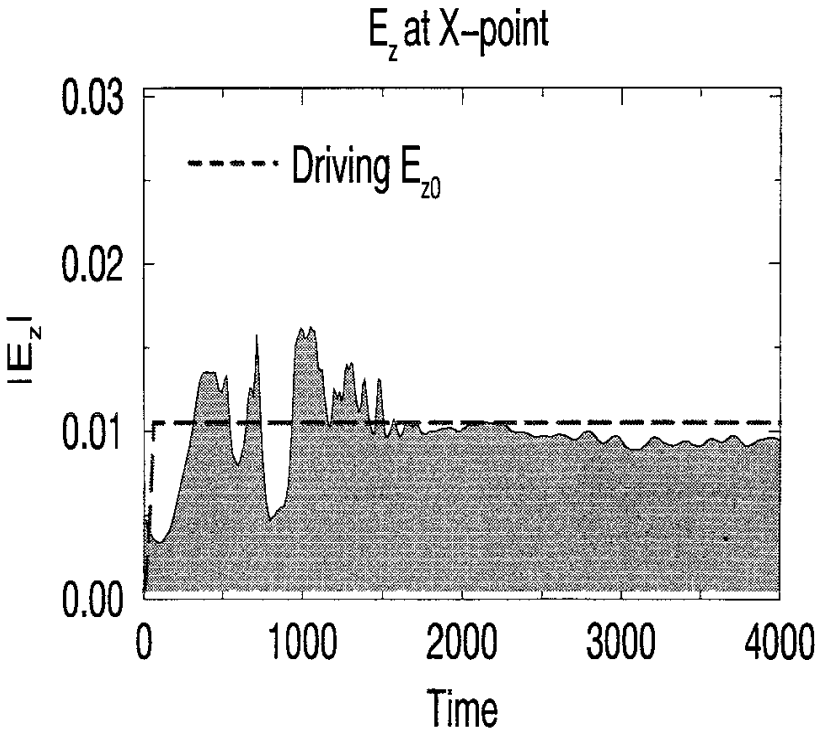
E_z at X-point
0.03
0.02
0.01
0.00
Driving E_z0
|E_z|
0
1000
2000
3000
4000
Time

Fig.14

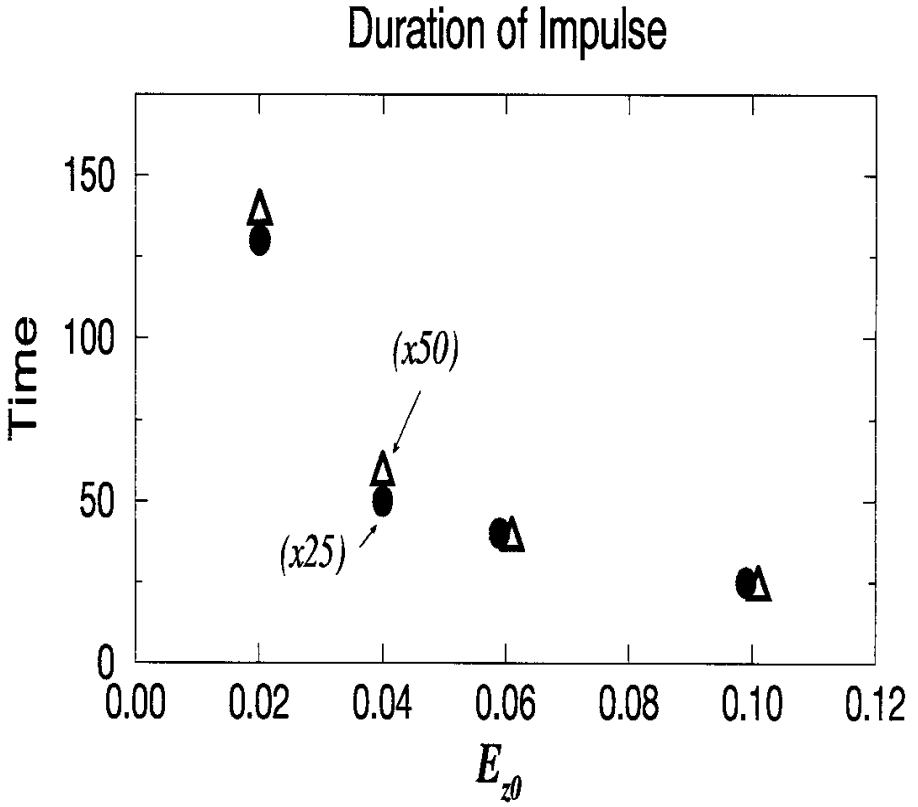
Duration of Impulse
Time
150
100
50
0
0.00
0.02
0.04
0.06
0.08
0.10
0.12
(x50)
(x25)
E_{z0}

Fig.15

Variable	Normalization unit
Magnetic field	B_{x0}
Plasma density	ρ_0
Spatial length	L
Velocity	$V_A \equiv B_{x0}/(\mu_0\rho_0)^{1/2}$
Time	L/V_A
Current	$B_{x0}/\mu_0 L$
Electric field	$B_{x0}V_A$
Pressure	$B_{x0}^2/2\mu_0$
Resistivity	$\mu_0 L V_A$
Viscosity	$\rho_0 L V_A$

Table 1

E_0	η	ν	γ	B_{z0}	P_1
0.06	5×10^{-3}	10^{-3}	2	0	10^{-2}

Table 2

Recent Issues of NIFS Series

NIFS-337 B.B.Kadomtsev,
Ball Lightning as Self-Organization Phenomenon; Feb. 1995

NIFS-338 Y. Takeiri, A. Ando, O. Kaneko, Y. Oka, K. Tsumori, R. Akiyama, E. Asano, T. Kawamoto, M. Tanaka and T. Kuroda,
High-Energy Acceleration of an Intense Negative Ion Beam; Feb. 1995

NIFS-339 K. Toi, T. Morisaki, S. Sakakibara, S. Ohdachi, T.Minami, S. Morita, H. Yamada, K. Tanaka, K. Ida, S. Okamura, A. Ejiri, H. Iguchi, K. Nishimura, K. Matsuoka, A. Ando, J. Xu, I. Yamada, K. Narihara, R. Akiyama, H. Idei, S. Kubo, T. Ozaki, C. Takahashi, K. Tsumori,
H-Mode Study in CHS; Feb. 1995

NIFS-340 T. Okada and H. Tazawa,
Filamentation Instability in a Light Ion Beam-plasma System with External Magnetic Field; Feb. 1995

NIFS-341 T. Watanbe, G. Gnudi,
A New Algorithm for Differential-Algebraic Equations Based on HIDM; Feb. 13, 1995

NIFS-342 Y. Nejoh,
New Stationary Solutions of the Nonlinear Drift Wave Equation; Feb. 1995

NIFS-343 A. Ejiri, S. Sakakibara and K. Kawahata,
Signal Based Mixing Analysis for the Magnetohydrodynamic Mode Reconstruction from Homodyne Microwave Reflectometry; Mar.. 1995

NIFS-344 B.B.Kadomtsev, K. Itoh, S.-I. Itoh
Fast Change in Core Transport after L-H Transition; Mar. 1995

NIFS-345 W.X. Wang, M. Okamoto, N. Nakajima and S. Murakami,
An Accurate Nonlinear Monte Carlo Collision Operator; Mar. 1995

NIFS-346 S. Sasaki, S. Takamura, S. Masuzaki, S. Watanabe, T. Kato, K. Kadota,
Helium I Line Intensity Ratios in a Plasma for the Diagnostics of Fusion Edge Plasmas; Mar. 1995

NIFS-347 M. Osakabe,
Measurement of Neutron Energy on D-T Fusion Plasma Experiments; Apr. 1995

NIFS-348 M. Sita Janaki, M.R. Gupta and Brahmananda Dasgupta,
Adiabatic Electron Acceleration in a Cnoidal Wave; Apr. 1995

NIFS-349 J. Xu, K. Ida and J. Fujita,
A Note for Pitch Angle Measurement of Magnetic Field in a Toroidal Plasma Using Motional Stark Effect; Apr. 1995

NIFS-350 J. Uramoto,
Characteristics for Metal Plate Penetration of a Low Energy Negative Muonlike or Pionlike Particle Beam: Apr. 1995

NIFS-351 J. Uramoto,
An Estimation of Life Time for A Low Energy Negative Pionlike Particle Beam: Apr. 1995

NIFS-352 A. Taniike,
Energy Loss Mechanism of a Gold Ion Beam on a Tandem Acceleration System: May 1995

NIFS-353 A. Nishizawa, Y. Hamada, Y. Kawasumi and H. Iguchi,
Increase of Lifetime of Thallium Zeolite Ion Source for Single-Ended Accelerator: May 1995

NIFS-354 S. Murakami, N. Nakajima, S. Okamura and M. Okamoto,
Orbital Aspects of Reachable β Value in NBI Heated Heliotron/Torsatrons; May 1995

NIFS-355 H. Sugama and W. Horton,
Neoclassical and Anomalous Transport in Axisymmetric Toroidal Plasmas with Electrostatic Turbulence; May 1995

NIFS-356 N. Ohyabu
A New Boundary Control Scheme for Simultaneous Achievement of H-mode and Radiative Cooling (SHC Boundary); May 1995

NIFS-357 Y. Hamada, K.N. Sato, H. Sakakita, A. Nishizawa, Y. Kawasumi, R. Liang, K. Kawahata, A. Ejiri, K. Toi, K. Narihara, K. Sato, T. Seki, H. Iguchi, A. Fujisawa, K. Adachi, S. Hidekuma, S. Hirokura, K. Ida, M. Kojima, J. Koong, R. Kumazawa, H. Kuramoto, T. Minami,. M. Sasao, T. Tsuzuki, J.Xu, I. Yamada, and T. Watari,
Large Potential Change Induced by Pellet Injection in JIPP T-IIU Tokamak Plasmas; May 1995

NIFS-358 M. Ida and T. Yabe,
Implicit CIP (Cubic-Interpolated Propagation) Method in One Dimension; May 1995

NIFS-359 A. Kageyama, T. Sato and The Complexity Simulation Group,
Computer Has Solved A Historical Puzzle: Generation of Earth's Dipole Field; June 1995

NIFS-360 K. Itoh, S.-I. Itoh, M. Yagi and A. Fukuyama,

Dynamic Structure in Self-Sustained Turbulence; June 1995

NIFS-361 K. Kamada, H. Kinoshita and H. Takahashi,
Anomalous Heat Evolution of Deuteron Implanted Al on Electron Bombardment; June 1995

NIFS-362 V.D. Pustovitov,
Suppression of Pfirsch-schlüter Current by Vertical Magnetic Field in Stellarators; June 1995

NIFS-363 A. Ida, H. Sanuki and J. Todoroki
An Extended K-dV Equation for Nonlinear Magnetosonic Wave in a Multi-Ion Plasma; June 1995

NIFS-364 H. Sugama and W. Horton
Entropy Production and Onsager Symmetry in Neoclassical Transport Processes of Toroidal Plasmas; July 1995

NIFS-365 K. Itoh, S.-I. Itoh, A. Fukuyama and M. Yagi,
On the Minimum Circulating Power of Steady State Tokamaks; July 1995

NIFS-366 K. Itoh and Sanae-I. Itoh,
The Role of Electric Field in Confinement; July 1995

NIFS-367 F. Xiao and T. Yabe,
A Rational Function Based Scheme for Solving Advection Equation; July 1995

NIFS-368 Y. Takeiri, O. Kaneko, Y. Oka, K. Tsumori, E. Asano, R. Akiyama, T. Kawamoto and T. Kuroda,
Multi-Beamlet Focusing of Intense Negative Ion Beams by Aperture Displacement Technique; Aug. 1995

NIFS-369 A. Ando, Y. Takeiri, O. Kaneko, Y. Oka, K. Tsumori, E. Asano, T. Kawamoto, R. Akiyama and T. Kuroda,
Experiments of an Intense H- Ion Beam Acceleration; Aug. 1995

NIFS-370 M. Sasao, A. Taniike, I. Nomura, M. Wada, H. Yamaoka and M. Sato,
Development of Diagnostic Beams for Alpha Particle Measurement on ITER; Aug. 1995

NIFS-371 S. Yamaguchi, J. Yamamoto and O. Motojima;
A New Cable -in conduit Conductor Magnet with Insulated Strands; Sep. 1995

NIFS-372 H. Miura,
Enstrophy Generation in a Shock-Dominated Turbulence; Sep. 1995

NIFS-373 M. Natsir, A. Sagara, K. Tsuzuki, B. Tsuchiya, Y. Hasegawa, O. Motojima, *Control of Discharge Conditions to Reduce Hydrogen Content in Low Z Films Produced with DC Glow;* Sep. 1995

NIFS-374 K. Tsuzuki, M. Natsir, N. Inoue, A. Sagara, N. Noda, O. Motojima, T. Mochizuki, I. Fujita, T. Hino and T. Yamashina, *Behavior of Hydrogen Atoms in Boron Films during H_2 and He Glow Discharge and Thermal Desorption;* Sep. 1995

NIFS-375 U. Stroth, M. Murakami, R.A. Dory, H. Yamada, S. Okamura, F. Sano and T. Obiki, *Energy Confinement Scaling from the International Stellarator Database*; Sep. 1995

NIFS-376 S. Bazdenkov, T. Sato, K. Watanabe and The Complexity Simulation Group, *Multi-Scale Semi-Ideal Magnetohydrodynamics of a Tokamak Plasma;* Sep. 1995

NIFS-377 J. Uramoto, *Extraction of Negative Pionlike Particles from a H2 or D2 Gas Discharge Plasma in Magnetic Field;* Sep. 1995

NIFS-378 K. Akaishi, *Theoretical Consideration for the Outgassing Characteristics of an Unbaked Vacuum System*; Oct. 1995

NIFS-379 H. Shimazu, S. Machida and M. Tanaka, *Macro-Particle Simulation of Collisionless Parallel Shocks*; Oct. 1995

NIFS-380 N. Kondo and Y. Kondoh, *Eigenfunction Spectrum Analysis for Self-organization in Dissipative Solitons;* Oct. 1995

NIFS-381 Y. Kondoh, M. Yoshizawa, A. Nakano and T. Yabe, *Self-organization of Two-dimensional Incompressible Viscous Flow in a Friction-free Box;* Oct. 1995

NIFS-382 Y.N. Nejoh and H. Sanuki, *The Effects of the Beam and Ion Temperatures on Ion-Acoustic Waves in an Electron Beam-Plasma System;* Oct. 1995

NIFS-383 K. Ichiguchi, O. Motojima, K. Yamazaki, N. Nakajima and M. Okamoto *Flexibility of LHD Configuration with Multi-Layer Helical Coils;* Nov. 1995

NIFS-384 D. Biskamp, E. Schwarz and J.F. Drake, *Two-dimensional Electron Magnetohydrodynamic Turbulence*; Nov. 1995